

Cite this: DOI: 10.1039/xxxxxxxxxx

When does near-wall hindered diffusion influence mass transport towards targets?[†]

Shaltiel Eloul^a, Enno Kätelhön^a, and Richard G. Compton^{*a}

Received Date
Accepted Date

DOI: 10.1039/xxxxxxxxxx

www.rsc.org/journalname

The diffusion of a particle is slowed as it moves close to a surface. We identify the conditions under which this hindered diffusion is significant and show that is strongly dependant on the sizes of both the particle and the target. We focus particularly on the transport of nano-particles to a variety of targets including a planar surface, a sphere, a disc and a wire, and provide data which allows the frequency of impacts to be inferred for a variety of experimental conditions. Equations are given to estimate the particle fluxes and we explain literature observations reported on the detected frequency of impacts. Finally we observe a drastic effect on the calculation of the mean first passage time of a single particle impacting a sub-micron sized target, showing the importance of this effect in biological systems.

1 Introduction

Predicting the events of single particles stochastically hitting a target by virtue of their Brownian motion is of great interest in understanding numerous biophysical and chemical processes. Over the past decade, growing attention has been given to processes involving single particles impacting[‡] on electrodes. This method enables the study of various types of individual particles such as metal nano-particles^{1–3}, biomolecules^{4–6} including bacteria⁷, and smaller particles such as agglomerates of C₆₀ molecules^{8,9}.

Particles are usually considered to diffuse freely in solution and stochastically impact at micro- or smaller electrodes^{3,10,11}. During an ‘impact’, the particle may undergo a direct charge transfer reaction or may mediate a reaction between the electrode and a solution phase species^{12,13}. A corresponding current in the form of a ‘spike’ can then be measured^{1,14}, which may provide direct information on the particle size distribution¹⁵. The average number of impacts as function of time and the individual particles’ first passage times of reaching the electrode can be described by the diffusion equation^{16,17}, on which basis models can be developed providing important tools to verify experiments

and to measure the concentration of nano-particles in ultra-dilute samples for example for environmental studies¹⁸. The impact method has recently opened new ways to identify and model nano-particle agglomeration in solution^{19–21}, to study chemical mechanisms^{4,6,22}, and to characterise the composition of modified nano-particles^{2,23}. In general, studying stochastic arrivals of particles to small targets and the mean first passage time of a single particle, is of large interest in many processes. These include the interaction of biological macromolecules²⁴ and nano-particles²⁵, modelling drug delivery²⁶, and in biological processes such as rate regulation²⁷.

The transport of particles, from bulk solution to a reaction zone close to the surface of a target is usually described solely by Brownian motion. Thus the frequency (impact s^{−1}) of observed impacts can be estimated by solving the diffusion equation:

$$\frac{\partial c}{\partial t} = \nabla \cdot (D \cdot \nabla c) \quad (1)$$

with mixed Dirichlet-Neumann boundary conditions for the adsorption at the surface of a small target, such as an electrode, and reflection elsewhere.

In bulk solution, each particle has a characteristic isotropic diffusion coefficient D_0 that reflects its size and shape. The Stokes-Einstein relation gives the bulk diffusion coefficient of a spherical particle in the limit of low Reynolds numbers, which is found to be a good estimation even for particles in water of radii r_p of only a few nanometres²⁸:

$$D_0 = \frac{k_B T}{6\pi\eta r_p} \quad (2)$$

where η is the dynamic viscosity, k_B is the Boltzmann constant,

* Corresponding Author.

^a Department of Chemistry, Physical and Theoretical Chemistry, Oxford University, South Parks Road, Oxford OX1 3QZ, United Kingdom.

[†] Electronic Supplementary Information (ESI) available: Includes details on the computational methods (1), the solution of the diffusion equation towards a sphere (2), further details on the anisotropic 2D diffusion equation (3), and discussion on the residual maps of the steady state flu equations (4). See DOI: 10.1039/b000000x/

[‡] In the context of particles diffusively arriving at an electrode, the term ‘impact’ is commonly used and thus we follow this convention in the text. In the literature this event is also described as a ‘collision’.

and T is the temperature. When the space available for diffusion is confined, the particle's hydrodynamic mobility must be taken into account when modelling its diffusive transport. Brenner²⁹ and Faxén³⁰ have calculated the corrections to the Stokes-Einstein relation for the normal- and parallel diffusion coefficients near a wall. The expressions agree well with experiments^{31,32}. Bevan and Prieve have approximated the analytical solution made by Brenner for the case of hindered diffusion normal to a wall for a sphere with a radius r_p , separated by a distance h :

$$D(h) = \frac{6h^2 + 2r_ph}{6h^2 + 9r_ph + 2r_p^2} \cdot D_0 \quad (3)$$

where h is the separation distance between the wall and the closest point of the particle surface. The same study reported an experiment to quantify diffusion coefficients of micro-beads at very close distances to walls. Using optical measurements they produced results that followed the above expression for a ratio of separation (h) to the particle radius, $h/r_p = 40\text{nm}/3.5\mu\text{m} \sim 0.01$. The hindering of diffusion due to space confinement (also referred to as "geometrically constrained Brownian motion") is also evident in porous media such as zeolites³³, and is crucial in various models of biological systems^{34,35} such as for the delivery of nanomedicine in the confined zone of a tumour rich in collagen³⁶.

When modelling the diffusive mass transport of particles from the bulk, far from any boundaries, to an active site on a surface, the effect of hindered diffusion is however often legitimately neglected in experimental studies. For instance, in nano-impact experiments, the observed mass transport of silver nano-particles showed good agreement with free diffusion without any consideration of hindered diffusion^{14,17}. Also, a previous model for diffusion towards a sphere showed only minor differences in comparison to experiments with nickel nano particles of radius 26 nm³⁷. On the other hand side, previous stochastic calculations of the duration of an impact event at an electrode showed the necessity of including hindered diffusion for predicting the residence time of an impact³⁸. Additionally, a very recent study modelled the case of a convection-diffusion system for a rotating electrode in a nano-impact experiment and showed that hindered diffusion significantly affects the flux towards a rotating electrode³⁹.

In this work, we show that when the target is small, hindered diffusion becomes important for the prediction of the particle flux and the estimation of the number of impacts in experiments. We show that this effect is due to convergent diffusion⁴⁰, where the diffusion field is confined to a small space near the surface (not centre) and regardless of the cell size. This confinement of the diffusion field defines the influence of hindered diffusion on the flux and first passage time of a particle searching for a target. The flux is estimated to be a function of the size of the target and its geometry. We provide approximate functions that can be used directly to estimate the flux of particles towards electrode. It is shown below that the effect becomes important for nano-particles searching for a target of the order of a micrometre or else.

The study has also importance for various nano-particle or macromolecule attachment models^{25,26}. Moreover, first passage statistics are important to understand biological processes such

as the synapse regulation of the exit rate through an ultra small window in a bounded domain²⁷ and how viruses travel towards a nuclear pore⁴¹. These types of diffusion problem are analogues to that examined below and known as the 'Narrow escape time' problem^{42,43}. It is shown here, that in such systems the estimation of the first passage time, is changed drastically as a function of the target size due to the hindering of diffusion.

In this paper, we first examine the importance of the effect on the steady state flux at small targets, by solving the diffusion equation for a simplified one-dimensional (1D) model. It is shown that the transport is strongly influenced by the hindering of diffusion in the case of sufficiently small targets. Then we provide the results of a numerical study for a variety of targets including spherical, disc and wire electrodes, and give approximate but applicable functions for the steady state flux and data for the expected number of impacts in various experimental conditions.

2 Simplified model

For the purpose of explaining when hindered diffusion has an influence on the diffusion flux, we examine the analytical solution of diffusion towards a small sphere. In the context of the 'nano-impact' approach, the size of the electrode must be small in order to minimize the occurrence of simultaneous impacts on the electrode and to reduce the capacitive noise so as to facilitate small charge measurements. Therefore micron-sized electrodes, or smaller, are commonly employed¹⁸. First, neglecting hindered diffusion, the diffusion equation results in Fick's second law in radial coordinates:

$$\frac{\partial c}{\partial t} = D_0 \left(\frac{\partial^2 c}{\partial r^2} + \frac{2}{r} \frac{\partial c}{\partial r} \right) \quad (4)$$

r is the radial coordinate with $r=0$ corresponds to the centre of the sphere. r_s is the sphere radius and a positive point in r direction. c is the number concentration (*particles/m³*). Along with the boundary conditions of a fully adsorbing sphere with the radius $r = r_s, c = 0$ and $r = r_\infty, c = c^*$ this solves to give^{40,44}:

$$c(r,t) = c^* \left[1 - \frac{r_s}{r} \operatorname{erfc} \left(\frac{r - r_s}{\sqrt{4D_0t}} \right) \right] \quad (5)$$

and the flux at the surface is:

$$-D_0 \frac{\partial c}{\partial r} \Big|_{r=r_s} = c^*(r_s, t_0) D_0 \left[\frac{1}{\sqrt{\pi D_0 t}} + \frac{1}{r_s} \right] \quad (6)$$

For the convenience of the reader, the derivation is supplied in Supplementary Information. The flux towards a sphere illustrates the convergent behaviour of the diffusion field. The time dependent term is dominant at short times and vanishes at larger time, whilst the $1/r_s$ term is size-dependent but constant with time. At large electrodes and practical time scales, the transient is dominant and the second convergent term can be neglected.

An insightful exercise to understand the influence of hindered diffusion on such a system is to add a distance-dependent diffusion coefficient in a form of a simplified function. This allows the analytical study of the hindered-diffusion effect on the flux. To this end, we use a simple function instead of the more complex

approximation given in eq. (3):

$$D_{trial}(r) = D_0 e^{-Br_s/r} \sim D(r) \quad (7)$$

where r is the distance between the centre of the sphere ($r = 0$) to the closest point of the particle surface. B is a fitting parameter that might be fitted to various r_p and has no units. The dimensional parameters are given in table 1. It can be seen in figure 1 that the function closely follows the Bevan's and Prieve's approximation for this purpose. For the simplicity of the present exercise, the function depends on the distance from $r=0$, the centre of the small sphere target. This means that the function is finite when $r_s/r = 1$ and not zero, thus is less valid for very small B (see also figure 1).

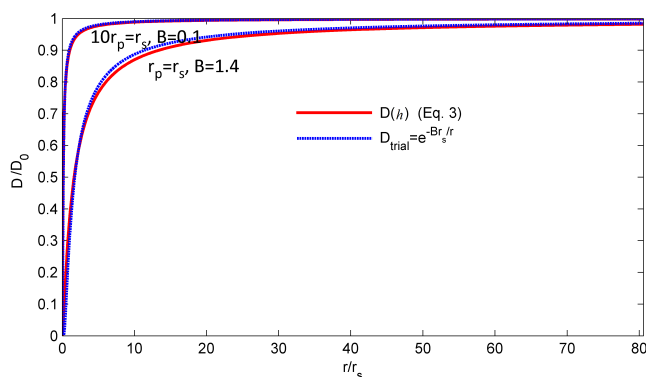


Fig. 1 Example of the behaviour of the approximate exponential function compared to $D(h)$ when $r_s = r_p \rightarrow B = 1.4r_s$ and $r_s = 10r_p \rightarrow B = 0.1r_s$. For simplicity of the model, the distance is taken from $r=0$ the centre of the small target.

Substitution of the function into the diffusion equation, and simplifying to steady state, the diffusion equation becomes:

$$0 = \frac{\partial^2 c}{\partial r^2} + \left(\frac{2}{r} + \frac{Br_s}{r^2} \right) \frac{\partial c}{\partial r} \quad (8)$$

By reducing order and substituting the boundary condition $c(x = 0, t) = 0$ and $c(x = \infty, t) = c^*$, the steady state flux (J_{ss}) solves to (see also Supporting Information):

$$J_{ss} = \frac{D_0 c^*}{r_s} \left[\frac{B}{(1 - e^B)} \right] \quad (9)$$

It can be seen that when $B \rightarrow 0$, (when the particle is very small relative to r_s), the term in the squared brackets tends to unity. This results in the same steady state current found for non-hindered mass transport (eq. 6). When B is greater than 0, the steady state flux decreases and at very large B ($B \rightarrow \infty$), the steady state flux tends to zero. *This shows that the effect of limited diffusion on the steady state flux strongly depends on the ratio r_p/r_s .* For example, when $r_s = r_p$, B is fitted to 1.4 and the steady state current is reduced to $0.45D_0c^*/r_s$, which is 45% of the steady state flux found without hindered diffusion. When $r_s = 10r_p$, however, the steady state flux is only reduced to 95 %, demonstrating that when the target is sufficiently large, hindered diffusion can be neglected in the steady state.

Table 1 Dimensional parameters

Parameter	Description	Units
r_p	Radius of a particle	m
r_c	Radius of a cell	m
r_d	Radius of a target disc	m
r_s	Radius of a target surface	m
r_w	Radius of a target wire	m
l	Length of a wire	m
L	Length of a 1D cell	m
D_0	Diffusion coefficient from the Stokes-Einstein eq.	$m^2 s^{-1}$
D	Diffusion coefficient, distance dependant	$m^2 s^{-1}$
c	Number concentration	$particles/m^3$
c^*	Bulk number concentration	$particles/m^3$
j	Flux density	$particles/(m^2 s)$
J_{ss}	Steady state flux	$particles/s$
τ_0	First passage time for non-hindered diffusion	s
τ_D	First passage time for hindered diffusion case	s
P_{impact}	Probability of impact	
N_{impact}	Average number of impacts	
X_t	Average tunnelling distance	m

3 Numerical study

The numerical study is divided into three parts. First, the results for a 1D and macro-scale target are reported in order to show in which cell size the contribution of hindered diffusion can be neglected as function of the particle size. Second, we present the results for the flux towards a small sphere in a cell of arbitrary size, and show a strong decrease in the flux which depends on the ratio between the particle size and the target size. We also report the drastic effect of the hindered diffusion on the first passage time calculations for very small targets. Third, the study of two important experimental systems is reported, the diffusion of particles towards a microdisc and a wire. An approximate function is provided to estimate the 2D anisotropic diffusion of particles towards a disc. We also explain why a relatively small effect is observed on a wire in comparison to the disc and sphere.

3.1 1D cell and a macro-scale target

The study of a 1D linear system is a starting point that shows the domination of near-wall hindered diffusion as function of a confined cell with a length L . The target is located at $x = 0$ and a fixed wall at $x = L$. The cell is schematically shown in figure 2. When a particle hits the target, a full adsorption is assumed. For instance, in the case of the 'impact' method, a high over-potential is applied on the electrode as a target and metal-particles that arrive by diffusion are fully oxidised. The cell in figure 2 shows the typical diffusion field (layer) that propagates from the adsorbing target and reaches the wall at long times. The non-homogeneous hydrodynamic loss is a particle size dependent function and assumed to be small in comparison to a macro-target, thus it is illustrated as a thin layer next to the adsorbing surface (figure 2). Additionally, we neglect the effect of hindered diffusion on the upper wall, though in a very small confined space this effect would be significant.

3.1.1 Model

The diffusion equation in 1D has the form:

$$\frac{\partial c}{\partial t} = \nabla \cdot (D(x) \cdot \nabla c) \quad (10)$$

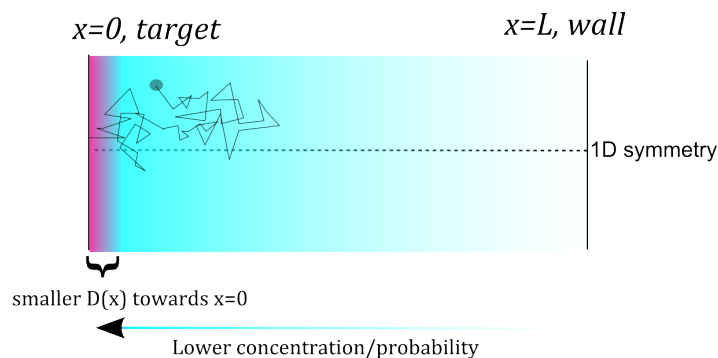


Fig. 2 Confined 1D geometry featuring a large targets. The drawing illustrates the diffusion field (cyan to white gradient) and the non-homogeneous reduction in the diffusion coefficient (violet to blue). Changes in the diffusion coefficient next to the upper wall ($x = L$) are neglected.

where $D(x)$ follows Bevan and Prieve approximation shown earlier (eq. (3)).

It is noted that the expression (eq. (3)) tends to zero at the surface of the wall. Moreover, at very small distances from the wall the continuous model is not valid due to surface attraction or repulsion forces, double layer interactions, or even the wall roughness³⁰. However, in a Faradaic reaction, the charge is transported from the surface of the particle to the electrode via electron tunnelling. Thus, we recognize an average tunnelling distance of the order of $X_t = 1$ nm, and locate the adsorbing boundary at this point^{37,45}, so that on this boundary, $c(x = X_t, t \geq 0) = 0$. As a result, the diffusion coefficient is finite on the adsorbing boundary. In the results below for the quantitative studies, we use an explicit expression for the tunnelling distribution function as is discussed later in this paper.

At the upper boundary we use a reflection boundary condition:

$$t \geq 0, \left. \frac{\partial c(x, t)}{\partial x} \right|_{x=L} = 0 \quad (11)$$

At $t=0$ the concentration is set to the initial concentration c^* . The flux is evaluated numerically through mass balance to avoid numerical errors in the calculation of the diffusion coefficient next to the wall:

$$J(t) = \int_{X_t}^L \frac{\partial c}{\partial t} dx \quad (12)$$

In the case of small cells, instead of presenting the flux of particles, it is more informative to calculate the cumulative probability of an impact from a single particle searching the adsorbing boundary in a finite cell:

$$P_{\text{impact}}(t) = c^* L - \int_{X_t}^L c(x, t) dx \quad (13)$$

where c^* is the initial probability density to find a single particle in size L and equals $1/L$. We solve the model numerically using the Implicit-Finite Difference Method which is detailed in the Supplementary Information.

3.1.2 Discussion

The results of the probability of an impact at different sizes of confined cells are presented in figure 3 for representative r_p of 100nm. The results are also compared to calculations of the ‘non-hindered’ case. It is shown that the effect becomes smaller as the cell gets larger, and negligible in cells which are above 100 μm in length.

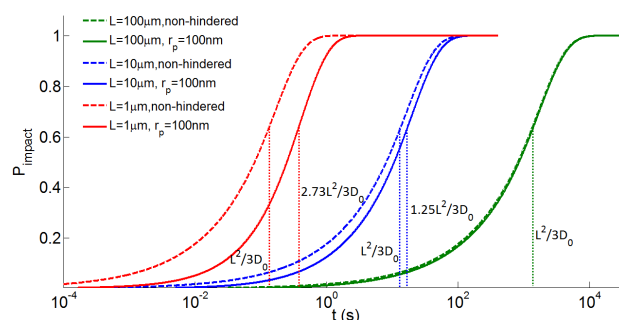


Fig. 3 The influence of hindered diffusion on the probability of impact, in a confined space for large targets and various cell sizes $L=100\mu\text{m}, 10\mu\text{m}, 1\mu\text{m}$. The dashed lines presents the non-hindered calculations, and the solid lines the calculations with hindered diffusion.

The analytical solution of the mean time for impact with no consideration of hindered-diffusion follows $L^2/3D$ in such a geometry[§]. We compare this value to the mean time of impact in the ‘hindered’ case which is calculated numerically (also referred to the ‘mean first passage time’)⁴⁶:

$$\tau_0 = \int_0^\infty \int_{X_t}^L [1 - c(x, t)] dx dt \quad (14)$$

As shown in figure 3. Only at very small $L = 1\mu\text{m}$, is a significant effect on the expected time of impact observed for the 100nm particles. It is concluded from these results that for a macro electrode as a target, the effect of hindered diffusion can be legitimately neglected unless the cell is confined to a very small size. This is easily explained by the fact that in a non-confined cell the diffusion layer gets much further away from the hindered diffusion zone and therefore most of the time the particle ‘searches’ for the target with a bulk diffusion coefficient (as illustrated in figure 2). Hence, the expectation time or the flux in a many-particle system are in such cases not much influenced by hindered diffusion. This behaviour is valid only in the case of large targets as discussed in the previous section. We next provide the calculations for the case of a finite sphere where near-wall hindered diffusion can play an important role regardless of the cell size.

3.2 1D cell - a finite sphere target

The diffusion of a particle towards a sphere is schematically shown in figure 4. In this case, the diffusion layer is convergent

[§] $L^2/3D$ is calculated directly from the integration of the mean passage time: $D_0 \Delta \tau(x) = -1$ with the boundary conditions, $\tau(0) = 0$ and $\partial_x \tau(L) = 0$, for a particle with a initial uniform probability density in all x (from 0 to L).

(also confined to a small distance), and depends on the particle size can be comparable to the hindered diffusion zone. As a result, the particle diffusion coefficient is hindered for a significant fraction of its searching time.

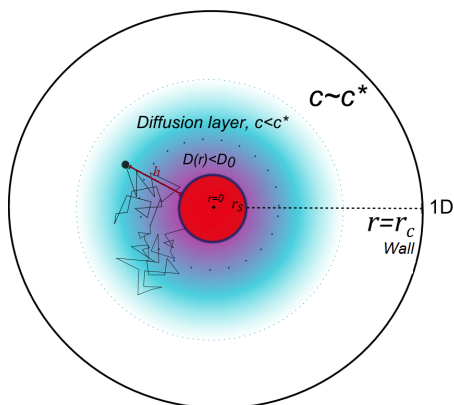


Fig. 4 Bounded cell of a size r_c with 1D radial symmetry (solid circle), featuring a finite sphere electrode as a target (r_s). The drawing illustrates the diffusion field/layer (cyan to white gradient, limited by the denser-dotted circle) and the hindered diffusion layer near the spherical target (violet to blue, limited by the space-dotted circle).

3.2.1 Model

We numerically solve the non-homogeneous diffusion equation in spherical coordinates and 1D radial symmetry:

$$\frac{\partial c(r,t)}{\partial t} = D(r-r_s) \left(\frac{\partial^2 c}{\partial r^2} + \frac{2}{r} \frac{\partial c}{\partial r} \right) + \frac{\partial D(r-r_s)}{\partial r} \frac{\partial c}{\partial r} - P \quad (15)$$

where $D(r-r_s)$ is the hindered diffusion coefficient calculated in accordance with eq. (3), where h equals $r-r_s$.

In order to get a better accuracy for very small targets and particle sizes, instead of using a fully adsorbing boundary, we use an electron tunnelling approximation via a sink term (P), to model the impact of a particle as a fast reaction at a very small distance from the surface. This follows an exponential fall off of the tunnelling probability with distance:

$$P = c(r,t) \nu e^{-\beta(r-r_s)} \quad (16)$$

ν is the tunnelling rate (s^{-1}) of the process which is chosen to be sufficiently large to provide a converged result. β is the electron decay factor (m^{-1}) which is solvent dependent and from scanning tunnelling microscope measurements is thought to be 1.59 \AA^{-1} in aqueous media^{45,47}. It is noted that our calculation is found to be insensitive to small changes in the value of this parameter, however the effect of the tunnelling distance is varies for various sizes of targets as is discussed next in the dimensionless analysis and in the result.

3.2.2 Dimensionless form

We can transform the diffusion equation into a dimensionless form in order to reduce the number of dependant parameters. The r coordinate, the particle radius, and the cell size are nor-

malised to the radius of the sphere:

$$R = r/r_s, R_p = r_p/r_s, R_c = r_c/r_s \quad (17)$$

A dimensionless time is introduced:

$$\tau = D_0 t / r_s^2 \quad (18)$$

and the diffusion coefficient and the concentration can be normalised to:

$$D^*(R) = D(R)/D_0 \quad (19)$$

$$C = c/c^* \quad (20)$$

This results in the dimensionless form of the diffusion problem:

$$\frac{\partial C}{\partial \tau} = D^*(R-1) \left(\frac{\partial^2 C}{\partial R^2} + \frac{2}{R} \frac{\partial C}{\partial R} \right) + \frac{\partial D^*(R-1)}{\partial R} \frac{\partial C}{\partial R} - P^* \quad (21)$$

where the dimensionless sink term is given as:

$$P^* = \frac{C r_s^2}{D_0} \nu e^{-\beta^*(R-1)} \quad (22)$$

and $\beta^* = \beta r_s$.

Reflection boundary conditions are used everywhere, at the surface of the electrode sphere and at the upper boundary of the cell.

The dimensionless total flux of particles impacting the sphere is calculated through the mass balance as follows:

$$J_0(\tau) = 4\pi \int_1^{R_c} \frac{\partial C}{\partial \tau} R^2 dR \quad (23)$$

The dimensional flux is therefore:

$$J(t) = J_0(\tau) c^* r_s D_0 \quad (24)$$

We carried out a full parametric study to quantify the time dependent and the steady state flux. Details on the numerical solution and convergence tests are provided in the computational methods (see Supplementary Information).

3.2.3 Discussion

The effect of hindered diffusion on the transient flux of particles for various ratios R_p (r_p/r_s) impacting on a sphere is shown in figure 5. In order to provide a clear estimation of the effect at different ratios (r_p/r_s), the flux is normalised to the theoretical steady state flux towards a sphere ($4\pi c^* r_s D_0$).

The results show a strong dependence of the expected flux on the ratio r_p/r_s . The results also suggest that the transient flux is strongly influenced by hindered diffusion at all times. At very short times this is due to the arrival of particles from very short distances, where $D(r) \ll D_0$. In contrast with the case of a macro-scale flat target, the steady-state flux strongly depends on the particle size.

Since β^* depends on r_s , β^* can also affect the flux response. Figure 6 shows the behaviour of the normalised flux of particles for various ratios r_p/r_s and for a large range of $\beta^* = 10^4 - 10^6$. The figure shows that the flux depends also on β^* and therefore

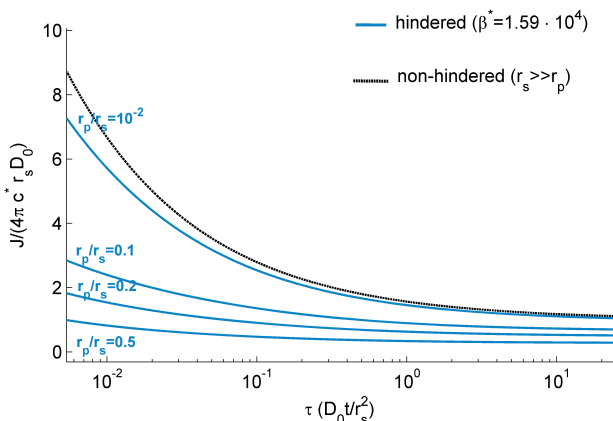


Fig. 5 Flux of particles of various R_p (r_p/r_s), normalised to steady state and as function of dimensionless time. $\beta^* = 1.59 \cdot 10^4$, which corresponds to $r_s = 1\mu\text{m}$ and $\beta = 1.59\text{\AA}^{-1}$ in aqueous media.

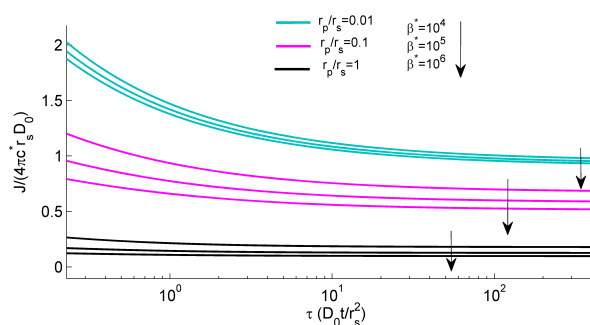


Fig. 6 Flux of particles of various R_p ($r_p/r_s=0.01, 0.1, 1$), and for various $\beta^* = 10^4, 10^5, 10^6$. The flux is normalised to steady state and as function of dimensionless time.

is a function of the absolute value of the tunnelling size. When the tunnelling distance is smaller (larger β^*), the effect of hindered diffusion layer is more dominant since the diffusion coefficient is damped to a lower value before charge transfer occurs. Accordingly, it is observed from the dimensionless analysis that for a given r_s/r_p , when r_s is larger, the flux is reduced and tends to be more affected by the hindered diffusion. Figure 6 also shows that when r_s/r_p is large (0.01) the effect of β^* is moderated. When the particle is very small relative to the target, the effect of hindered diffusion is reduced since the hindered diffusion layer becomes comparable in size to the size of the tunnelling zone.

For practical use, we also present the results using dimensional sizes of r_s and r_p . The effect of hindered diffusion on the transient flux of particles impacting on a sphere is shown in figure 7. In order to provide a clear estimation of the effect at different sizes of electrodes and particles, the flux is normalised to the theoretical steady state flux of each case, and the time is given in dimensionless units.

The results show a large reduction of the expected flux for 100nm particles and a moderate effect on the flux of 20nm particles. The effect found to be significant for target sizes in the order of $1\mu\text{m}$ and below.

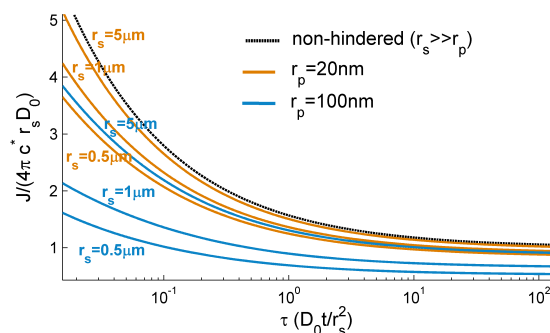


Fig. 7 Flux of particles of radius 20nm (orange curves) and 100nm (blue curves) normalised to steady state and as function of dimensionless time.

In many systems for single particle detection such as the ‘impact’ method, the diffusive flux of particles is at steady state. We have conducted a parametric study of the steady state flux (J_{ss}), to find the correlation between the size of the target and the particle size. The map of the flux relative to the flux under non-hindered diffusion was simulated for a set of 4000 parameters and is given in figure 8. We use the least-square method to fit the steady state flux map to an exponential function, relying on the behaviour found earlier, and the knowledge of the asymptotic solutions ($r_p/r_s \rightarrow \infty, J \rightarrow 0$ and $r_p/r_s \rightarrow 0, J \rightarrow 1$). The steady state equation in the case of particles impacting a sphere can be approximated as:

$$\text{sphere: } J_{ss,D(r)}^{fit} = 4D_0\pi c^* r_s (0.57e^{-2.34\frac{r_p}{r_s}} + 0.43e^{-0.21\frac{r_p}{r_s}} \pm Er) \quad (25)$$

The equation is fitted with an r-square value of 0.996, and can be used to estimate of the effect of hindered diffusion towards a sphere. The function provides a good fitting for most ratios of r_p/r_s , with a maximum deviation $Er = \pm 0.08$. We provide a residual map for better accuracy in the Supplementary Information. The equation along with the residual map can be used directly to estimate the flux of particles towards a sphere or a hemi-sphere.

The map in figure 8 and eq. (25) show the strong relation of the hindered diffusion as function of the ratio r_p/r_s . It is also shown that the effect is significant for micrometre targets and large nano-particles of a few hundreds nanometre sizes.

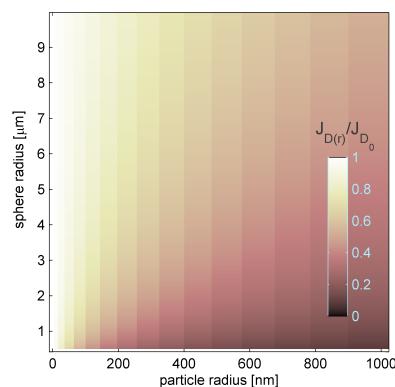


Fig. 8 The steady state flux map as a function of the nano-particle and sphere size.

Note that the results of the map presented in figure 8 and eq. (25) hold when the target is large in comparison to the particle size. When the particle size is comparable or larger than the target, the hydrodynamic mobility is less influenced by the target and would result in a deviation from the calculated steady state flux.

We next address the result of the mean first passage time (MFPT) of a particle searching for a sphere, bounded in a spherical cell of the order of a few micrometres. In such cells the target can be of the sub-micron size. This is relevant for biological processes involve with calculations the mean first passage times of a biomolecules searching for small targets^{41,42} and also relevant for small targets as nano-electrodes¹¹. We calculate the MFPT directly through the temporal integration of the survival density function:

$$\tau_D = \int_0^\infty [1 - 4\pi \int_{r_s}^{r_c} c(r,t) r^2 dr] dt \quad (26)$$

for one particle in a bounded sphere with radius r_c . We carried out a parametric study to find how the MFPT changes under the influence of near-wall hindered diffusion. For all cases we selected $r_c = 100r_s$, far enough from the target. The ratio between the calculation of the MFPT for non-hindered case τ_0 to the calculation of the 'hindered' case $\tau_{D(r)}$ are presented in the colour-map in figure 9. The map shows the deviation from the mean first passage time can be significant. For instance, when the target is in the order of a few hundreds nanometres, even considering a small radius of particle, such as 20nm, the expected MFPT is five times smaller than the calculated with including the hindered diffusion. The map shows that the first passage time can be reduced drastically for small targets even when considering the problem of small nano-sized particles searching for small targets.

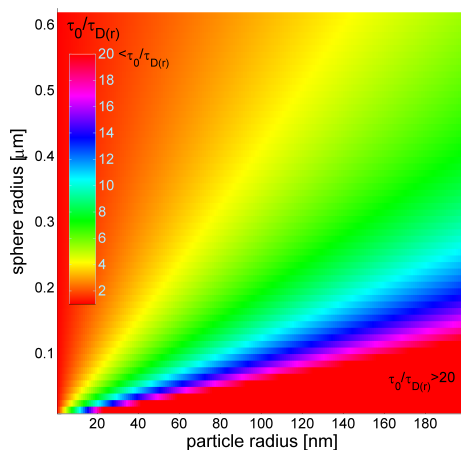


Fig. 9 The mean first passage time (MFPT) of a particle searching for a sphere for the 'non-hindered' case relative to the MFPT of the 'hindered' case.

4 Near-wall Hindered diffusion of particles towards a finite disc and a wire

In impact experiments or in general in sensing applications, microdisc or wire target¹⁸ geometries are generally used. These

behave as fully adsorbing surfaces in the case of electrodes when a sufficiently high potential is applied. The number of expected impacts in these systems is determined from the diffusion flux. Here we quantify the deviation from the expected flux as function of the disc radius or the wire radius in comparison to the particle size.

4.1 Hindered diffusion of particles towards a finite disc

Microdisc electrodes are typically fabricated by insulating a metal wire with a radius r_d of the order of microns in a glass sheath with a radius r_c . The 2D symmetry is illustrated in figure 10.

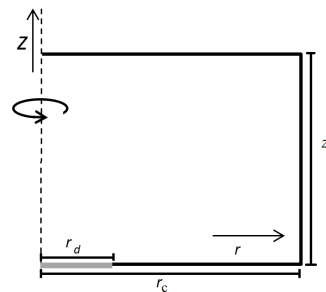


Fig. 10 Microdisc electrode with a radius r_d insulated with a sheath of a size $r_c (\gg r_d)$ in a cell size of $z_c (\gg r_d)$.

When particles arrive close to the surface of the sheath the hydrodynamic mobility loss is anisotropic in the normal (\hat{z}) and parallel directions (\hat{r}). In cylindrical coordinates, the diffusion equation has the form⁴⁸:

$$\frac{\partial c}{\partial t} = \nabla \cdot \left\{ D \cdot \left(\frac{\partial c}{\partial r} \hat{r} + \frac{1}{r} \frac{\partial c}{\partial \phi} \hat{\phi} + \frac{\partial c}{\partial z} \hat{z} \right) \right\} \quad (27)$$

and the diffusion coefficient is represented by a second rank tensor:

$$D = D_0 \begin{bmatrix} \sigma_{rr} & \sigma_{r\phi} & \sigma_{rz} \\ \sigma_{\phi r} & \sigma_{\phi\phi} & \sigma_{\phi z} \\ \sigma_{zr} & \sigma_{z\phi} & \sigma_{zz} \end{bmatrix} \quad (28)$$

For an axisymmetric system like the ones considered, the anisotropic diffusion equation simplifies to:

$$\frac{\partial c}{\partial t} = D_0 \left(\sigma_{rr} \frac{\partial^2 c}{\partial r^2} + \frac{\sigma_{rr}}{r} \frac{\partial c}{\partial r} + \sigma_{zz} \frac{\partial^2 c}{\partial z^2} + \frac{\partial \sigma_{zz}}{\partial z} \frac{\partial c}{\partial z} \right) - P \quad (29)$$

More detail is provided in the Supporting Information). $\sigma_{zz}(z)$ follows the Bevan and Prieve approximation (eq. (3)) and for the parallel diffusion coefficient, $\sigma_{rr}(z)$, Faxén's approximation can be used³⁰:

$$\sigma_{rr}(h) = 1 - \frac{9}{16} \left(\frac{r_p}{h+r_p} \right) + \frac{1}{8} \left(\frac{r_p}{h+r_p} \right)^3 - \frac{45}{256} \left(\frac{r_p}{h+r_p} \right)^4 - \frac{1}{16} \left(\frac{r_p}{h+r_p} \right)^5 \quad (30)$$

Anisotropic diffusion in this system is considered for the disc and for the insulating sheath surrounding it. Hindered diffusion for

the cell boundaries far from the electrodes is neglected. Instead of using an adsorbing boundary on the disk, we add a sink term P as is discussed for the case of a sphere. Here we implement the electron tunnelling zone as a function of the distance z from the surfaces. Reflection boundary conditions are considered everywhere, on the insulating sheath, on the cell boundaries, and on the disk electrode. The cell boundaries in the case of the microdisc are generally far enough to affect diffusion in the time scale of experiment. Invariably, we chose r_c and z_c to be larger than $6\sqrt{D_0 t}^{40}$. At zero time, the concentration in all space is set to the bulk concentration, $c(x, t = 0) = c^*$.

We solve the 2D anisotropic diffusion equation numerically (see methods in Supplementary Information) and to calculate the flux and the accumulated number of impacts on a microdisc surface through mass balance. The value of β selected is $\beta = 1.59\text{\AA}^{-1}$ and therefore assume that the zone of electron transferring is tiny in comparison to the size of the hindered diffusion layer and diffusion layer. The effects of hindered diffusion on the transient flux and the number of impacts on a micro-disc are presented in figure 11a and figure 11b, respectively. In order to provide a clear estimation of the effect at different sizes of electrodes and particles, the flux is normalised to $J/(c^* r_s D_0)$, and the time is in dimensionless units (tD_0/r_s^2). The number of impacts in 11b is further normalized to $c^* r_s^3$. The transient curves for the different sizes of targets and for 100nm and 20nm sizes are compared to the flux for non-hindered case. The results show the different behaviour of the flux and the expectation of the number of impacts is influenced by the disc size in the case of particle of 100nm but only a moderate deviation is expected for small size nano-particles, even at ultra-small electrodes.

The result explains the fit to Fick's diffusion (non-hindered case) of experimental measurements to determine concentrations of silver nano-particles and for Nickel nano-particles via $6.9\mu\text{m}$ microdisc electrodes¹⁴. In their work, the frequency of impacts was measured for various dilute concentrations, and found to increase linearly with the concentration. Moreover, for each concentration they fitted the accumulative number of impacts to the theoretical number of impacts from Fick's diffusion which was found to be with good agreement (less than 5% deviation in a 5s measurement).

The result shows an example of the importance of this analysis for the determination of nano-particles in environmental applications.

We examined further the steady-state response by a parametric study in a similar way as discussed for the sphere. The colour map of the ratio between the steady state flux to the steady-state flux in non-hindered case is presented in figure 12. We also assume $\beta = 1.59\text{\AA}^{-1}$ and show the result for the dimensional case where r_s and r_p is varied. The map shows no significant differences from the sphere case. This is due to the fact that the solution for a sphere is also the solution of hemisphere lying on a large reflecting surface which closely resembles the case of the disc⁴⁹. However, the steady state flux is found to be fitted to a similar function with different coefficients:

$$\text{disc: } J_{ss,D(r)}^{fit} = 4D_0 c^* r_d (0.57e^{-3.37 \frac{r_p}{r_s}} + 0.43e^{-0.26 \frac{r_p}{r_s}} \pm Er) \quad (31)$$

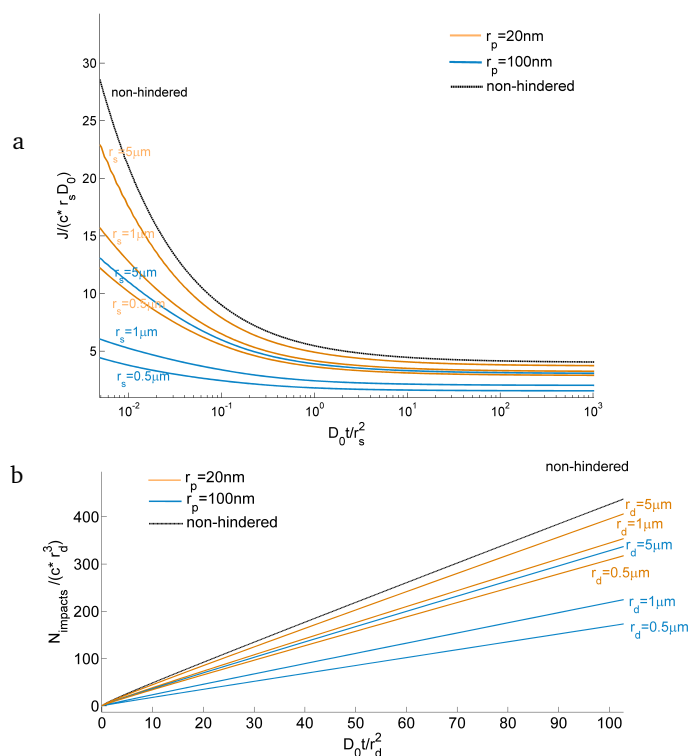


Fig. 11 The influence of hindered diffusion on the normalised flux (a), and on the number of impacts expected (b) on a microdisc target for various disc radii ($0.5\mu\text{m}$ - $5\mu\text{m}$), and for particles of 20nm (orange curves) and 100nm (blue curves). The dashed & black curves represent the cases of neglecting hindered diffusion. β is chosen to be 1.59\AA^{-1} .

The goodness of the fitting (r-square=0.9943) is shown by the residual map (Er) in the Supplementary Information. The functions along with the residual map can also be used directly by experimentalist for the prediction of the hindered diffusion effect on the flux of particles and for an estimation of the number of impacts.

Examining the coefficients of the exponentials in the functions of the spherical case in eq. (25) (-2.34,-0.21) and the disc case (-3.37,-0.26) reveals the contribution of the anisotropic transport. The significantly larger coefficients for the disc function indicates a stronger reduction of the flux in comparison to the steady state flux. This is due to the additional hydrodynamic loss in the lateral direction (r) when a particle arrives at the sheath surface.

Note that for the disc as a target, the size of the wall that hinders the hydrodynamic mobility is the size of the target as well as the usually large insulating sheath. Therefore, the model holds also when the target size is comparable to the size of the particle.

4.2 Hindered diffusion towards a wire

An important case is the wire electrode recommended for use in particle impact experiments consists of micro-sized radius r_w and length l , typically $l \gg r_w$. The wire electrode geometry has provides a higher number of impacts for the same electrode area of a disc¹⁶. In addition, impact experiments of large particle sizes, usually only become feasible with wire electrodes^{7,18}. Here we

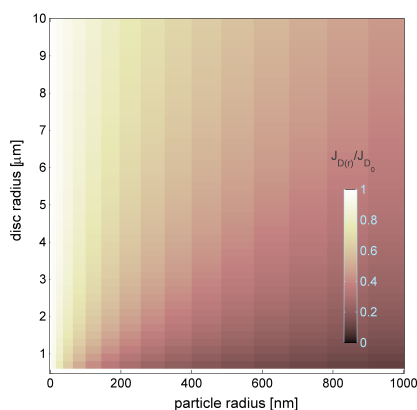


Fig. 12 The hindered diffusion steady state flux as a fraction of the non-hindered flux ($J_{D(r)}/J_{D0}$) map as a function of the nano-particle size and the disc size. The map present the case of $\beta = 1.59\text{\AA}^{-1}$.

can show that the effect of near-wall hindered diffusion is much reduced in comparison to the case of a sphere or disc due to the changed characteristic diffusion field towards the wire. The diffusion layer characterised with a mixed behaviour of small and large scale targets. The diffusion equation can be solved by assuming axial symmetry; we will neglect edge effects in our treatment. The diffusion equation is therefore:

$$\frac{\partial c(r,t)}{\partial t} = D(r-r_w) \left(\frac{\partial^2 c}{\partial r^2} + \frac{1}{r} \frac{\partial c}{\partial r} \right) + \frac{\partial D(r-r_w)}{\partial r} \frac{\partial c}{\partial r} - P \quad (32)$$

where r_w is the micro-size radius of the wire. We use the same methodology and boundary conditions described earlier in the sphere case.

The results for the number of impacts for various sizes of particles are presented for $1\mu\text{m}$ and for $5\mu\text{m}$ radii in figure 13a and figure 13b, respectively. The number of impacts is normalized to $2\pi c^* l r_w^2$. The results can easily be converted for experimental purposes. The curves show a significantly reduced effect of hindered diffusion in comparison with the disk or sphere as targets. This is due to the semi ‘macro’ behaviour of the wire. The diffusion layer propagates into a much larger space than in the case of fully convergent diffusion due to the large length of the wire. We hence find that the number of impacts is less influenced by hindered diffusion.

This observation explains the surprising high number of impacts reported for large particles (E.coli bacteria)⁷ of size $>1.0\mu\text{m}$ impacting a wire electrode with a radius of $3.5\mu\text{m}$. A frequency of $\sim 0.25\text{s}^{-1}$ which is $\sim 60\%$ of the expected frequency from pure Fickian diffusion was reported. This observation agrees with the calculated average frequency with the inclusion of hindered diffusion $\sim 0.21\text{s}^{-1}$ for a $1\mu\text{m}$ particle size (for simplicity approximating the bacteria a spherical particle). This proportion can also be inferred by looking at figure 13b for the case of $5\mu\text{m}$. The lower calculated frequency can be related to the fact that the bacteria size ($>1.0\mu\text{m}$) is in the order of the size of the wall ($3.5\mu\text{m}$).

It is also useful to discuss the result of the dimensionless form

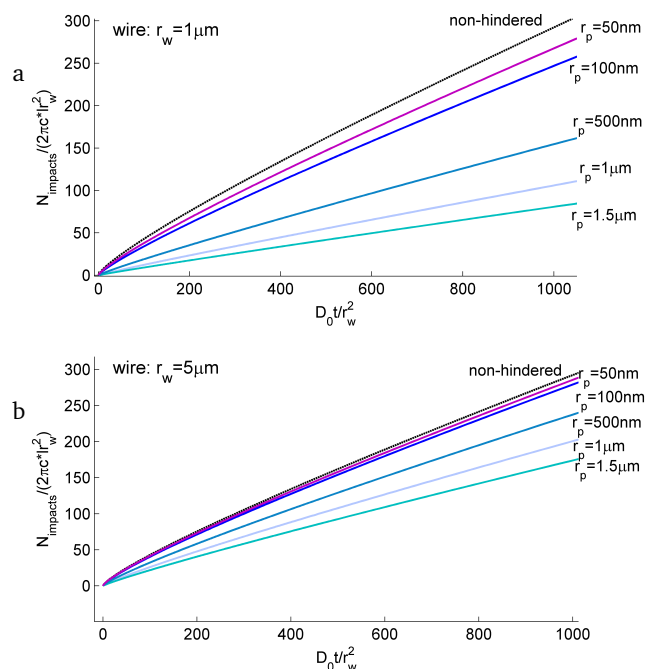


Fig. 13 The number of impacts expected on a wire for various sizes of particles (50nm- $1.5\mu\text{m}$) compared to the ‘non-hindered’ case. The results are presented for a wire of a radius $r_w = 1\mu\text{m}$ (a), and $r_w = 5\mu\text{m}$ (b), $\beta = 1.59\text{\AA}^{-1}$.

problem, in the same manner it is discussed earlier for the sphere. In this case the coordinates are normalised to r_w , so the diffusion equation becomes:

$$\frac{\partial C}{\partial \tau} = D^*(R-1) \left(\frac{\partial^2 C}{\partial R^2} + \frac{1}{R} \frac{\partial C}{\partial R} \right) + \frac{\partial D^*(R-1)}{\partial R} \frac{\partial C}{\partial R} - P^* \quad (33)$$

$$P^* = \frac{C r_w^2}{D_0} \text{ve}^{-\beta^*(R-1)} \quad (34)$$

and $\beta^* = \beta r_w$.

Figure 14 shows the normalised flux towards the wire for two different ratios $r_p/r_w = 0.01, 0.1$ and as function of β^* . The results show that the effect of β^* , (a measure of the tunnelling distance) on the flux is smaller at small ratios as observed in the case of the sphere. However, it is also observed that the effect of β^* on the flux is reduced strongly at long time. This is due to the reduced effect of the hindered diffusion layer towards a wire.

5 Conclusions

When a particle diffuses from bulk solution towards a target it is slowed close to the target. We have shown that although in a non-confined space hindered diffusion can be legitimately neglected, for sufficiently small targets the transport is effectively confined by the diffusion field. Subsequently, the flux strongly depends on the size of the particle and the size of the target regardless of the cell size. The numerical study have also shown a significant reduction of the flux at targets of the order of a micrometre, and particularly for particles of the order of 100nm or larger.

Parametric studies have enabled the development of equations that show the flux dependency on the ratio between the size of

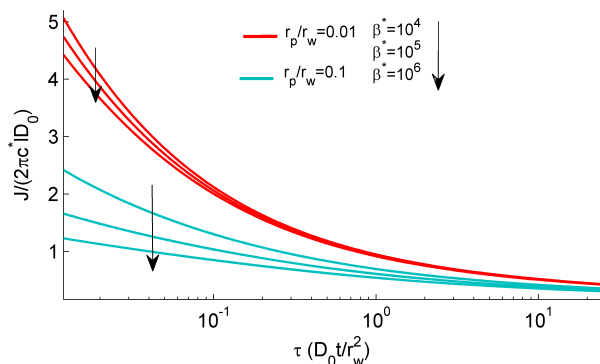


Fig. 14 Flux of particles of various R_p (r_p/r_w) and β^* . The flux is normalised to steady state and presented as a function of dimensionless time.

the target and the size of the particle assuming that the zone of hindered diffusion is larger than that of electron transfer. The functions estimate the flux of particles in experimental studies such as of the electrochemical ‘impact’ method and can be used to estimate the stochastic number of impacts.

For instance, the calculation of ‘impacts’ towards a wire target as an electrode could explain the high number of particle impacts despite the large size of particles. The later agrees with the calculated average frequency of E.coli bacteria with the inclusion of hindered diffusion ($\sim 0.21\text{s}^{-1}$). The results also explain the close fitting to pure Fickian diffusion with a bulk diffusion coefficient of silver nano-particles and for Nickel nano-particles at a $\sim 7\mu\text{m}$ microdisc.

Additionally, calculations of the mean first passage time towards a sphere and a hemi-sphere have shown a large deviation from the non hindered case. We found that when the window is in the order of hundreds nanometers, the expected mean first passage time is five times shorter than the calculated hindered diffusion for a particle of a size of 20nm. Hence it is particularly important for the understanding of diffusion processes such as of biomolecules searching for sub-micrometre size targets. This includes synapse regulation of the exit rate, drug delivery applications and modelling viruses travel towards a nuclear pore.

6 Acknowledgements

We thank Yavor Novev for helpful discussions and insightful comments. The research leading to these results has received funding from the European Union’s Seventh Framework Programme (FP/2007- 2013)/ERC Grand Agreement n. [320403].

References

- 1 Y.-G. Zhou, N. V. Rees and R. G. Compton, *Angew. Chem., Int. Ed.*, 2011, **50**, 4219–4221.
- 2 N. P. Sardesai, D. Andreescu and S. Andreescu, *J. Am. Chem. Soc.*, 2013, **135**, 16770–16773.
- 3 N. V. Rees, Y.-G. Zhou and R. G. Compton, *RSC Adv.*, 2012, **2**, 379–384.
- 4 T. M. Alligant, E. G. Nettleton and R. M. Crooks, *Lab Chip*, 2013, **13**, 349–354.
- 5 J. E. Dick, A. T. Hilterbrand, A. Boika, J. W. Upton and A. J. Bard, *Proceedings of the National Academy of Sciences*, 2015, **112**, 5303–5308.
- 6 W. Cheng and R. G. Compton, *Angew. Chem., Int. Ed.*, 2014, **53**, 13928–13930.
- 7 L. Sepunaru, K. Tschulik, C. Batchelor-McAuley, R. Gavish and R. G. Compton, *Biomaterials Science*, 2015, **3**, 816–820.
- 8 M. Pumera, *ACS Nano*, 2014, **8**, 7555–7558.
- 9 E. J. E. Stuart, K. Tschulik, C. Batchelor-McAuley and R. G. Compton, *ACS Nano*, 2014, **8**, 7648–7654.
- 10 X. Xiao and A. J. Bard, *J. Am. Chem. Soc.*, 2007, **129**, 9610–9612.
- 11 F.-R. F. Fan and A. J. Bard, *Science*, 1997, **277**, 1791–1793.
- 12 E. Kätelhön and R. G. Compton, *ChemElectroChem*, 2015, **2**, 64–67.
- 13 A. J. Bard, H. Zhou and S. J. Kwon, *Israel Journal of Chemistry*, 2010, **50**, 267–276.
- 14 E. J. E. Stuart, Y.-G. Zhou, N. V. Rees and R. G. Compton, *RSC Adv.*, 2012, **2**, 6879–6884.
- 15 W. Cheng and R. G. Compton, *TrAC Trends in Anal. Chem.*, 2014, **58**, 79 – 89.
- 16 S. Eloul, E. Kätelhön, C. Batchelor-McAuley, K. Tschulik and R. G. Compton, *J. Electroanal. Chem.*, 2015, **755**, 136–142.
- 17 A. Boika and A. J. Bard, *Analytical Chemistry*, 2015, **87**, 4341–4346.
- 18 J. Ellison, C. Batchelor-McAuley, K. Tschulik and R. G. Compton, *Sensor Actuat B-Chem*, 2014, **200**, 47 – 52.
- 19 K. Tschulik and R. G. Compton, *Phys. Chem. Chem. Phys.*, 2014, **16**, 13909–13913.
- 20 D. Qiu, S. Wang, Y. Zheng and Z. Deng, *Nanotechnology*, 2013, **24**, 505707.
- 21 S. V. Sokolov, E. Kätelhön and R. G. Compton, *J. Phys. Chem. C*, 2015, **119**, 25093–25099.
- 22 H. Zhou, F.-R. F. Fan and A. J. Bard, *J. Phys. Chem. Lett.*, 2010, **1**, 2671–2674.
- 23 L. R. Holt, B. J. Plowman, N. P. Young, K. Tschulik and R. G. Compton, *Angew. Chem., Int. Ed.*, 2016, **55**, 397–400.
- 24 K. Pappaert, P. V. Hummelen, J. Vanderhoeven, G. Baron and G. Desmet, *Chemical Engineering Science*, 2003, **58**, 4921 – 4930.
- 25 V. P. Zhdanov and F. Höök, *European Biophysics Journal*, 2015, **44**, 219–226.
- 26 F. Danhier, O. Feron and V. Préat, *Journal of Controlled Release*, 2010, **148**, 135–146.
- 27 A. Singer, Z. Schuss and D. Holcman, *Phys. Rev. E*, 2008, **78**, 051111.
- 28 J. T. Edward, *Journal of Chemical Education*, 1970, **47**, 261.
- 29 H. Brenner, *Chemical Engineering Science*, 1961, **16**, 242–251.
- 30 A. Goldman, R. Cox and H. Brenner, *Chemical Engineering Science*, 1967, **22**, 653–660.
- 31 P. Huang and K. S. Breuer, *Phys. Rev. E*, 2007, **76**, 046307.
- 32 M. A. Bevan and D. C. Prieve, *J. Chem. Phys.*, 2000, **113**, 1228–1236.

- 33 J. Karger and D. M. Ruthven, *Diffusion in Zeolites and Other Microporous Solids*, Wiley, New York, 1992, pp. 42, 90.
- 34 S. L. Dettmer, S. Pagliara, K. Misiunas and U. F. Keyser, *Phys. Rev. E*, 2014, **89**, 062305.
- 35 S. Pagliara, C. Schwall and U. F. Keyser, *Advanced Materials*, 2013, **25**, 844–849.
- 36 R. K. Jain and T. Stylianopoulos, *Nature Reviews Clinical Oncology*, 2010, **7**, 653–664.
- 37 E. O. Barnes, Y.-G. Zhou, N. V. Rees and R. G. Compton, *J. Electroanal. Chem.*, 2013, **691**, 28–34.
- 38 E. Katelhon and R. G. Compton, *Chem. Sci.*, 2014, **5**, 4592–4598.
- 39 S. V. Sokolov, E. Kätelhön and R. G. Compton, *The Journal of Physical Chemistry C*, 2016, **120**, 10629–10640.
- 40 R. G. Compton and E. Banks, *Understanding Voltammetry (2nd Edition)*, Imperial College Press, London, UK, 2011, p. 157.
- 41 D. Holcman, *Journal of Statistical Physics*, 2007, **127**, 471–494.
- 42 Z. Schuss, A. Singer and D. Holcman, *Proceedings of the National Academy of Sciences*, 2007, **104**, 16098–16103.
- 43 O. Bénichou and R. Voituriez, *Phys. Rev. Lett.*, 2008, **100**, 168105.
- 44 A. J. Bard and L. Faulkner, *Electrochemical Methods: Fundamentals and Applications*, John Wiley and Sons, 2001, p. 180.
- 45 P. P. Edwards, H. Gray, M. Lodge and R. J. Williams, *Angew. Chem., Int. Ed.*, 2008, **47**, 6758–6765.
- 46 P. L. Krapivsky and S. Redner, *Am. J. Phys.*, 1996, **64**, 546–551.
- 47 M. Hugelmann and W. Schindler, *Surface Science*, 2003, **541**, L643–L648.
- 48 R. B. Bird, *Applied Mechanics Reviews*, 2002, **55**, R1–R4.
- 49 K. B. Oldham and C. G. Zoski, *Journal of electroanalytical chemistry and interfacial electrochemistry*, 1988, **256**, 11–19.